Title

Carboxymethyl cellulose-alginate interpenetrating hydroxy ethyl methacrylate crosslinked polyvinyl alcohol reinforced hybrid hydrogel templates with improved biological performance for cardiac tissue engineering.

Journal

Biotechnology and Bioengineering, 120(3)

Authors

Sedighim, Sharona

Chen, Yiqing

Xu, Changlu

et al.

Publication Date

2023-03-01

DOI

10.1002/bit.28291

Peer reviewed

Published in final edited form as:

Biotechnol Bioeng. 2023 March ; 120(3): 819–835. doi:10.1002/bit.28291.

Carboxymethyl cellulose-alginate interpenetrating hydroxy ethyl methacrylate crosslinked polyvinyl alcohol reinforced hybrid hydrogel templates with improved biological performance for cardiac tissue engineering

Sharona Sedighim[1], **Yiqing Chen**[2], **Changlu Xu**[2], **Rohit Mohindra**[1], **Huinan Liu**[2], **Devendra K. Agrawal**[1], **Finosh G. Thankam**[1,*]

[1]Department of Translational Research, Western University of Health Sciences, Pomona, California 91766, USA

[2]Department of Bioengineering, University of California, Riverside, CA 92521, USA

Abstract

Cardiac tissue engineering is an emerging approach for cardiac regeneration utilizing the inherent healing responses elicited by the surviving heart using biomaterial templates. In this study, we aimed to develop hydrogel scaffolds for cardiac tissue regeneration following myocardial infarction (MI). Two superabsorbent hydrogels, CAHA2A and CAHA2AP, were developed employing the interpenetration chemistry. CAHA2A was constituted with alginate, carboxymethyl cellulose, (hydroxyethyl) methacrylate (HEMA), and acrylic acid, where CAHA2AP was prepared by interpenetrated CAHA2A with polyvinyl alcohol (PVA). Both hydrogels displayed superior physiochemical characteristics, as determined by AT-IR spectral analysis, DSC measurements, tensile testing, contact angle, water profiling, dye release, and conductivity. In vitro degradation of the hydrogels displayed acceptable weight composure and pH changes. Both hydrogels were hemocompatible, and biocompatible as evident by direct contact and MTT assays. The hydrogels promoted anterograde and retrograde migration as determined by the z-stack analysis using H9c2 cells grown with both gels. Additionally, the co-culture of the hydrogels with swine epicardial adipose tissue (EAT) cells and cardiac fibroblasts resulted in the synchronous growth without any toxicity. Also, both hydrogels facilitated the production of extracellular matrix by the H9c2 cells. Overall, the findings support an appreciable in vitro performance of both hydrogels for cardiac tissue engineering applications.

[*]**Corresponding author:** Finosh G Thankam Ph.D., Department of Translational Research, College of Osteopathic Medicine of the Pacific, Western University of Health Sciences, 309 E. Second Street, Pomona, California 91766-1854, USA, Tel: Off: 909-469-7042, FThankam@westernu.edu.

Author contributions

SS: Conceptualization; experimental design, data generation; data analysis; manuscript preparation; manuscript editing. **YC**: experimental design, data generation; data analysis; manuscript editing. **CX**: experimental design, data generation; data analysis; manuscript editing. RM: data generation; data analysis; manuscript editing. **HL**: Conceptualization; experimental design, manuscript preparation; manuscript editing; resources. **DA**: Conceptualization; experimental design, manuscript preparation; manuscript editing; resources; funding. **FT**: Conceptualization; experimental design, data generation; data analysis; manuscript preparation; manuscript editing; resources; funding.

Conflict of intrest

The authors declare no competing interests.

Graphical Abstract

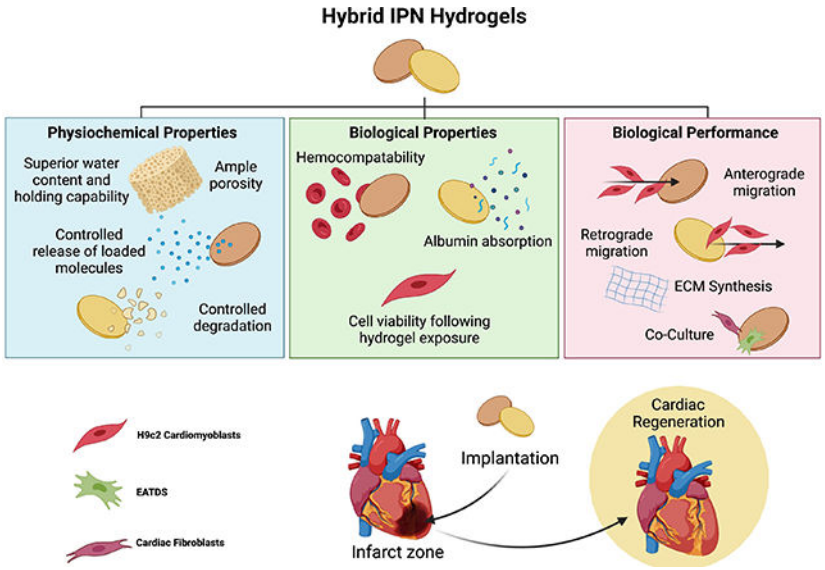

Keywords

Cardiac Tissue Engineering; IPN Hydrogels; Myocardial Infarction; Biocompatibility; Superabsorbent hydrogel

Introduction

Heart failure (HF) followed by myocardial infarction (MI) is one of the leading causes of death in the United States, affecting more than 6.2 million Americans (~ 2.4% of the population) over the age of 20 years, with the increasing rate of onset with age (Tsao et al., 2022). Alarmingly, the prevalence of MI is projected to increase to 46% by 2030 in individuals over the age of 18 years (Heidenreich et al., 2013). Risk factors for MI include hypertension, diabetes mellitus, smoking, and obesity accounting for 52% incidence of this disease (Dunlay et al., 2009). The permanent solution for MI is heart transplantation; however, extremely limited donor availability, and the increased rate of rejection (~24.10% in a 1-year follow up) are challenging (Gustafsson and Rogers, 2017; Minicucci et al., 2011). Mechanical circulatory support system devices including left ventricular assist devices (LVADs) have been employed as a bridge to transplantation for increased life expectancy. In addition, pharmacological medications (ACE inhibitors, ß-blockers, Angiotensin-II receptor blockers), coronary revascularization, implantable cardioverter-defibrillators, and cardiac resynchronization therapies have been used to support the patients; however, they pose several disadvantages (Bahit et al., 2018; Rana et al., 2015; Vaduganathan et al., 2020).

Due to the limitations in the conventional treatment approaches for end-stage cardiac failure, hydrogel-based tissue engineered implants have been proposed as alternative models for cardiac tissue regeneration. Hence, cardiac tissue engineering (CTE) aims to accelerate the cardiac healing using in vitro engineered tissue mimetics simulating the

native cardiac tissue (Rana et al., 2015). Biomaterial templates simulating the cardiac extracellular matrix (ECM) are inevitable in successful CTE where the hydrogel scaffolds gained prior significance owing to the close resemblances with native ECM providing an aqueous micro niche with excellent mass transfer abilities (Gnanaprakasam Thankam and Muthu, 2013). Moreover, such biodegradable hydrogels provide an ideal physiochemical and biological environment for adherence, proliferation, and differentiation of the cells of interest promoting cardiac repair (Thankam and Muthu, 2014a). Additionally, the porous network of the hydrogels facilitates the bidirectional (anterograde and retrograde) migration of cells (both the seeded and host) improving cardiac regeneration (Thankam and Muthu, 2014b). Interestingly, multiple approaches have been explored for engineering the hydrogels using natural and synthetic biomaterials, despite the advantages and disadvantages of the parent biomaterial (Li and Guan, 2011). The hydrogels formulations have used synthetic materials such as poly-ethylene glycol (PEG), poly-2-hydroxyethyl methacrylate (PHEMA), and polyamides and natural materials including collagen and decellularized ECM, fibrin, and matrigel (Li and Guan, 2011). Also, the polysaccharide alginate-based hydrogels have been commercially available for various biomedical and tissue engineering applications owing to their water kinetics, elasticity and biocompatibility. For instance, NU-GEL™ and Purilon® gel (alginate reinforced with carboxymethyl cellulose) are promising in ECM regeneration and re-epithelization accelerating the wound healing responses (Aswathy et al., 2020). However, the information on commercially available hydrogels for cardiac application is limited in the literature. Also, an ideal hydrogel satisfying the features of cardiac ECM is currently unavailable. Hence, in this study we designed and engineered a panel of interpenetrating network (IPN) hybrid hydrogels using the natural polysaccharides carboxymethyl cellulose (CMC), and alginate, and the synthetic co-monomers hydroxyethyl methacrylic acid (HEMA) and acrylic acid (AA) exploiting the interpenetration chemistry. The study investigated the in vitro performance of CMC-Alginate-HEMA-AA (CAHA) based hydrogels for CTE applications.

Materials and Methods

Materials

In the preparation and testing of hydrogels, the following chemicals and solutions were used: Alginate (Alginic acid sodium salt from brown algae, Cat#1003084114), sodium phosphate dibasic (Na_2HPO_4) (Cat#102200878), polyvinyl alcohol (PVA) (Cat#1003119330), acrylic acid (AA) (Cat#1002952044), calcium chloride ($CaCl_2$) (Cat#1002922361), L-ascorbic acid (Cat#1003083974), and ammonium persulfate (APS) (Cat#1003048376) were obtained from Sigma Aldrich. Additionally, PKH26 Red Fluorescent Cell Linker Mini Kit (MINI26-1KT) and PKH67 Green Fluorescent Cell Linker Mini kit (MINI67-1KT) were obtained from Sigma Aldrich for cell labelling. Carboxymethylcellulose (CMC) (Cat#217277) and 2-hydroxyethyl methacrylate (HEMA) (Cat#8.00588.0250) were purchased from EMD. Rhodamine Phalloidin (Cat#R415), Hoechst 33342 (Cat#1924445), and MTT (Cat#M6494) were purchased from Invitrogen. DMEM High Glucose with L-Glutamine (Cat#30-2002) was purchased from ATCC for cell culture media preparation. 10% Neutral Buffered Formalin (Cat#16004-128) was obtained from VWR for sample fixation. Dimethyl sulfoxide (DMSO) (Cat#196055) was purchased from mpbio, and Vetashield HardSet antifade

mounting medium with DAPI (Cat#H-1500) was obtained from Vector Laboratories. Pierce bicinchoninic acid (BCA) protein assay kit (Cat#23225) was obtained from ThermoFisher Scientific.

Synthesis of hydrogel scaffolds

HEMA and acrylic acid (AA) were allowed to undergo free-radical induced polymerization in alginate-CMC blend to form CMC-Alginate-HEMA-AA IPN hydrogel which was designated as CAHA2A. The alginate fraction was subjected to ionic crosslinking using divalent calcium and HEMA was subjected to vinyl polymerization using ascorbic acid/APS system ensuring the interpenetration. Briefly, sodium alginate solution (5%) was uniformly dispersed in Na_2HPO_4 (5%) followed by mixing CMC (0.5%). The blend was warmed to 60–70°C with constant stirring, followed by the addition of HEMA, AA, $CaCl_2$ (0.5%), L-ascorbic acid (10%), and APS (10%) and the mixture was casted for 1–2 days at 50–60°C to obtain a sheet of hydrogel. The sheet was then submerged into $CaCl_2$ (10%) for one hour for additional crosslinking of alginate fractions, washed in distilled (DI) water overnight, freeze dryed, UV sterilized, and stored aseptically in air-tight containers for further studies. Similarly, CAHA2A was reinforced with PVA (5%) prior to the casting to fabricate CAHA2A-PVA (CAHA2AP) IPN. Hence, the interpenetration was facilitated by calcium-alginate fragments and acrylic acid crosslinked HEMA chains whereas the CMC and PVA were entangled in the network via physical interactions (Figure 1).

Physicochemical Characterization

AT-IR—AT-IR spectral analysis was performed on freeze dried hydrogel discs to determine the surface functionality.

3D Imaging—The surface topography of freeze dried samples were imaged using a 3D laser microscope (VK-X150, Keyence, USA).

Scanning electron microscopy—The microstructures of the CAHA2A and CAHA2AP were characterized using a scanning electron microscope (SEM) (Nova NanoSEM 450, FEI Co.) at an accelerating voltage of 10 kV. Energy-dispersive X-ray spectroscopy (EDX) was performed at an accelerating voltage of 10 kV, and spot size of 3, using the X-Max 50 silicon drift detector attached to the SEM to determine the elemental composition of the samples. Aztec Energy software (Oxford Instruments, Abingdon, Oxfordshire, U.K.) was used to calculate the elemental composition and distribution. The images were processed using ImageJ software to quantify the pore dimension following our previous report (Gnanaprakasam Thankam and Muthu, 2014).

Differential scanning calorimetry—The hydrogels were imbibed in distilled water overnight for differential scanning calorimetry (DSC 214, Netzsch). Briefly, the CAHA2A (10 mg) and CAHA2AP (6.57 mg) samples were placed in the aluminum container associated with the instrument whereas empty container was used as a reference. The samples were cooled from 0°C to −40°C, then heated to 100°C at the rate of 5 K/min to record the heating and cooling curves. DSC analysis was performed in a protective N_2 atmosphere with an N_2 flow rate of 60 mL/min. The freezing free water and bound water

were calculated from the enthalpy of melting endotherm following our previously reported protocol (Finosh et al., 2015).

Contact angle—Freeze-dried hydrogel sheets of dimension 1cm x 3 cm with average weight of 18.6 mg and 12.3 mg and average thickness of 0.231 mm and 0.147 mm, respectively for CAHA2A and CAHA2AP, were assessed for surface hydrophilicity using the contact angle measurement. The advancing and receding contact angle were determined in distilled water using Wilhelmy method in KSV sigma 701 tensiometer (KSV Instruments Ltd, USA) (Finosh et al., 2015).

Water profiling—CAHA2A and CAHA2AP hydrogels were imbibed in distilled water to determine swelling kinetics, swelling ratio (S), equilibrium water content (EWC) and equilibrium swelling ratio (ESR) following our previous protocols (Thankam et al. 2022).

$$Swelling\ ratio\ (S) = \frac{M_t - M_0}{M_0}$$

$$\%Swelling\ (\%S) = \frac{M_f - M_0}{M_0}$$

$$ESR\left(E\right) = \frac{M_f - M_0}{M_f}$$

$$EWC = \frac{M_f - M_0}{M_f} \times 100$$

The swelling kinetics was determined by the extent of swelling at regular time intervals of 5 minutes employing the following formula (Thankam et al., 2022a). M_t represented the weight of the swollen hydrogel at time “t”, M_0 was the dry weight, and M_f is the mass of the swollen hydrogel in equilibrium. The diffusion of water molecules onto the interstices of the hydrogels were determined using following equation where E s ESR, S is the swelling ratio, K is the swelling constant, n is the diffusional exponent, and t is the time interval for swelling measurements.

$$\frac{S}{E} = Kt^n$$

K and n were obtained by the intercept and slope, respectively, from the plot of log(S/E) vs log(time). For CAHA2A hydrogels, this equation was

$$y = -0.003\ln(x) + 0.975$$

while the equation for CAHA2AP hydrogels was

$$y = \ -0.014\ln(x) + 0.9131$$

The total water absorption sites (TWAS) of the hydrogel were determined by the following equation where m is the molecular mass of one water molecule, 2.99×10^{-23}.

$$TWAS = \frac{M_f \ - \ M_0}{m}$$

Mechanical characterization

Mechanocompatibiility was assessed by the tensile strength of CAHA2A and CAHA2AP using the universal testing machine (Instron 5969 dual-column testing system) equipped with a 10 N load cell (Instron, Norwood, MA). The tensile testing was performed with 0.005 N preload using a crosshead speed of 5 mm/min and the experiments were conducted for five replicates for each sample (Finosh and Jayabalan, 2015).

Release kinetics

CAHA2A and CAHA2AP hydrogels were swollen overnight in hydrophobic dye trypan blue 5 mg% (n = 6) and hydrophilic dye methylene blue 50 mg% (n = 6). The release profile of the dyes was determined in 10 ml Ringer's solution (pH 7.30) at one hour interval for 8 hours followed by once daily for 21 days by replacing with 1 ml fresh Ringer's solution. The concentration of the released dyes was determined using the standard curve. Additionally, the cumulative percentage release was determined following an established protocol (Zin at al., 2020)

$$Release\ (\%) = \frac{Ab_0 \ - \ Ab_t}{Ab_0} \times 100$$

Where Ab_0 is the dye solution's initial absorbance and Ab_t is the dye solution's absorbance at time t.

Electrical conductivity

Water swollen hydrogels (n=6) were placed on a non-conductible surface and the electrical activity was measured using conductivity meter.

Biodegradation

In vitro degradation of the hydrogels was determined by aging in serum free DMEM containing 10% antibiotics (pH 7.80), at 37°C. Alterations in dry weight and pH were assessed at one week interval for a period of 4 weeks.

Hemocompatibility

Hemolysis assay—Blood was collected in anticoagulated tubes from Yucatan microswine (*Sus scorfa*, Sinclair bioresources) with prior approval by the IACUC of the Western University of Health Sciences, Pomona, CA. The blood was spun at 2000 rpm for 10 minutes to isolate red blood cells (RBC) and diluted in sterile PBS at 1:9 ratio. The samples were incubated with the RBC at 37°C for one hour. The RBCs incubated with distilled water and PBS were used as comparison controls. Following incubation, samples were centrifuged at 300g for 10 minutes, and the absorbance of the supernatant measured at 541 nm and the percentage hemolysis was calculated following our previous protocols (Finosh et al., 2015).

RBC aggregation—Smears of the above mentioned samples were prepared and observed under bright field microscope to assess the physical changes in the RBCs and rouleau formation (Finosh et al., 2015).

Protein adsorption—Freeze-dried, UV-sterilized hydrogels were incubated in 10% FBS (in sterile PBS) at 37°C overnight. The loosely bound proteins adsorbed onto the hydrogels were washed with sterile PBS, vigorously vortexed in 200μl PBS, centrifuged to remove the hydrogel debris and the protein content in the supernatant was quantified by bicinchoninic acid (BCA) assay (ThermoFisher). Protein adsorbed on the cell culture plate was used as the control. The extent of serum albumin adsorption onto the hydrogels was determined by SDS-PAGE using albumin as reference, and relative protein concentration was determined from band intensity using ImageJ software (Gnanaprakasam Thankam and Muthu, 2013).

Cytocompatibility

Cell culture and maintenance—Rat cardiomyoblast cells, H9c2(2–1) (Cat# CLR1446, ATCC) were used for the cytocompatibility and cell survival evaluations. The cells were maintained in high glucose DMEM with 10% fetal bovine serum (FBS) (Cat# 30–2020, ATCC) under the standard culture conditions (5% CO_2, 37°C, and antibiotics). Epicardial adipose tissue (EAT) was harvested from post-mortem Yucatan micro-swine and EAT-derived stem cells (EATDS) were isolated using collagenase digestion method and characterized following our previous protocol (Thankam and Agrawal, 2022). Similarly, cardiac fibroblasts (CF) were isolated from the left ventricular myocardium. EATDS and CF were maintained in high glucose DMEM containing 10% FBS and 20% FBS respectively as mentioned above. Upon 70–80% confluency the cells were split using standard trypsin method.

Direct contact assay—DMEM swollen hydrogels discs were placed on a sub-confluent monolayer of H9c2 cells, allowed to grow overnight, and their morphology upon contact with the hydrogels was assessed through imaging under an inverted phase contrast microscope (Olympus CKx41) following ISO-10993 standards as reported previously (Thankam and Muthu, 2014b). The survival of H9c2 cells grown on contact with the hydrogels was quantified using MTT cell viability assay as previously reported (Thankam et al., 2022a).

Test on extract—The hydrogels were extracted in complete DMEM for 48 hrs and the H9c2 cells were cultured overnight using DMEM extracts. The cell viability was quantified by MTT assay as mentioned above.

Biological Performance

Long term viability—H9c2 cells (5.98×10^6 cells/ml) were seeded onto DMEM swollen hydrogels, allowed to adhere for 45 min under standard culture conditions, followed by the addition of 3 ml culture media carefully onto the walls of the wells without disturbing the adhered cells, and incubated for 24 hours. The cell-laden hydrogels were transferred to new culture plates and allowed to grow for 15 days. The cells on the hydrogels were incubated with MTT (1 mg/ml) for 3 hours at 37°C, 0.1% HCl in isopropanol was added, vigorously vortexed for 20 min, centrifuged at 10,000 rpm to remove the debris and the absorbance of the supernatant was measured at 540 nm. Long-term viability was assessed at 5, 10, and 15-days post-gel transfer. H9c2 cells grown on culture plates and treated in similar manner were used as the control.

Anterograde cell migration—H9c2 cells (4.87×10^6 cells/ml) were seeded onto hydrogels as described above, and after 24 hours the H9c2-laden hydrogels were transferred to a new 12 well culture plate. The cells migrating from the hydrogel interface were carefully imaged daily using phase contrast microscope without disturbing the gels until full confluency. Additionally, the cell migration from CAHA2A and CAHA2AP scaffolds was evaluated using trans-well plates. H9c2 cells-laden hydrogels were placed into the upper chamber of trans-well plates with the surface containing cells facing toward the membrane. Top were filled with serum free medium and the bottom wells contained complete culture medium. Samples were incubated for 3 days and the membranes were stained for nuclei using DAPI and imaged using fluorescence imaging (Leica Thunder) to assess the cell migration.

Retrograde cell migration—H9c2 cells were labelled with viable fluorescent dye PKH67 to study the retrograde migration using the commercially available labeling kit (Sigma-Aldrich, MINI67–1KT) following the manufacturer's instructions. Briefly, H9c2 cells were pelleted and resuspended in diluent solution provided with the kit followed by the addition of PKH67 dye at a 1:1 ratio with the cell solution. The mixture was incubated at 37°C for 5 minutes, followed by addition of culture media to stop the reaction, washed three times with sterile PBS to remove excess dye, and resuspended in complete culture media prior to seeding. The labelled cells were seeded as mentioned before and the retrograde migration was determined using the fluorescent slide scanner microscope (Leica Thunder) using Z-stack mode. The 2.5 μm stacks were taken and penetration depth was calculated automatically using the LASX software associated with the microscope. The experiments were conducted in triplicate.

Cell spreading

The spreading of H9c2 cells in the interstices of CAHA2A and CAHA2AP hydrogels was examined three days after seeding using rhodamine staining kit following the manufacturer's instructions. Briefly, the hydrogels were fixed in formalin, blocked with 1% HBS, and

stained with Rhodamine Phalloidin (Invitrogen) for two hours. The gels were washed and the nuclei was counter-stained with Hoechst (Invitrogen) and imaged as mentioned before. The cells grown on cell culture plates were used as control.

ECM Synthesis

Aniline blue staining—H9c2 cells (1.35×10^6 cells/ml) were grown onto CAHA2A and CAHA2AP hydrogels for 2 days, fixed in formalin then stained with aniline blue for three min, washed with distilled water to remove excess stain, fixed with 1% acetic acid for 1 min, washed with distilled water, and dried overnight. The extent of collagen deposition was imaged using a brightfield microscope (Leica Thunder). The cells grown on glass coverslips were used as control. Similarly, the hydrogels were prepared as mentioned above and the ECM deposition was quantified using direct red assay following 5, 10, and 15 days post-seeding. Briefly, the hydrogels were removed from the media, washed with distilled water, incubated with 0.1% in 0.1M sodium hydroxide (NaOH) for one hour at room temperature, washed 4–5 times with 0.1M HCl, vortexed in 2M NaOH, vigorously vortexed, centrifuged at 10,000 rpm for 10 minutes and the absorbance of supernatant was measured at 540 nm.

Co-culture of CF and EATDS

EATDS and CF cells were isolated from swine heart tissue and maintained as described above. EATDS cells were labelled with PKH67 (green) and the CF cells were labelled with PKH26 (red) following the protocols mentioned above. EATDS (3.52×10^6 cells/ml) and CF (2.98×10^6 cells/ml) were suspended in 100μl complete culture media and seeded onto the hydrogels. Following incubation for 3 days, the hydrogels were washed with serum free media, mounted with DAPI and imaged using fluorescent microscopy (Leica Thunder) using Z-stack scanning (7.1μm stacks) and 3D rendering. The cells grown on glass coverslips were used as control.

Statistical analysis

The results of all conducted experiments were expressed as mean ± SEM. ImageJ software was used for pore measurements, DSC area calculations, and SDS Page absorption. The statistical significance was determined by unpaired ‘t’ test for comparing two groups and one-way ANOVA with two-stage linear step-up procedure of Benjamini, Krieger and Yekutieli test was employed for multiple comparison using GraphPad Prism software. Statistical significance of $P<0.05$ was set for all experiments.

Results

Synthesis of CAHA2A and CAHA2AP IPN hydrogels

The CAHA2A hydrogel scaffold was synthesized by blending the marine heteropolysaccharide alginate with the cellulose derivative CMC and HEMA with respective crosslinking of alginate with Ca^{++} and HEMA with AA using the APS/ascorbic acid redox initiator cocktail. The immediate gelling potential of alginate was controlled by optimizing the system with Na^+ ions allowing the casting and subsequent sheet formation. The CMC fraction was held by physical interaction of bulky alginate chains and the vinyl

crosslinked HEMA. Additional interpenetration was imparted in the CAHA2A system by reinforcing with PVA to form CAHA2AP. Additional crosslinking of the alginate segments was imparted by surplus Ca^{++} ions ensuring effective interpenetration in both CAHA2A and CAHA2AP hydrogels (Figure 1).

Physiochemical characterization

AT-IR—AT-IR spectrum analysis of the CAHA2A (n=6) and CAHA2AP (n=6) hydrogels revealed a broad peak around 3250 cm^{-1} (area of 1440.88 ± 186.96 for CAHA2A and 3543.56 ± 304.44 for CAHA2AP), suggesting the presence of -OH groups constituted by alginate and CMC in CAHA2A as well as PVA segments in CAHA2AP. The peak around 1590 cm^{-1} (area of 668.38 ± 112.56 for CAHA2A and 765.08 ± 195.23 for CAHA2AP) represented alkene C=C stretching suggesting the uncrosslinked HEMA segments. The peak around 1420cm^{-1} (area of 358.87 ± 41.75) in CAHA2AP revealed the -OH bending of PVA. The sharp peak around 1040cm^{-1} (area of 2119.57 ± 255.22 for CAHA2A and 2306.09 ± 660.27 for CAHA2AP) reflected the C-O-C stretching of the glycoside linkages in alginate, and CMC and PVA. The minor peak around 860 cm^{-1} (area of 386.43 ± 18.43) in CAHA2AP showed C-H bending in alginate, CMC and PVA. The peak around 1700 cm^{-1} (area of 550.06 ± 128.35) in CAHA2AP revealed carbonyl stretching of alginate. Hence, the IR spectral analysis revealed the presence of alginate, HEMA, PVA and CMC segments on the surface of respective CAHA2A and CAHA2AP scaffolds (Figure 2A and 2B). Also, the area of peaks revealed the increased level of functional groups in CAHA2AP than CAHA2A.

3D morphology—High resolution laser microscopy revealed irregular and uniformly distributed nano-features in both the CAHA2A and CAHA2AP hydrogels. The 3D laser microscopy revealed the surface roughness of CAHA2A and CAHA2AP hydrogels (Figures 2C–2F) where the CAHA2A displayed increased roughness compared to CAHA2AP. The ultra-morphology examination by SEM revealed surface morphology and inner porosity where the pores were homogenous with an average ratio of length-to-breadth (aspect ratio) 1.38 ± 0.075 μm and 1.40 ± 0.07 μm in CAHA2A and CAHA2AP hydrogels, respectively (*P=0.6796*) (Table 1). Also, no considerable difference in aspect ratio between the CAHA2A and CAHA2AP was observed (Figures 2G and 2J). The cross-sectional view displayed highly interconnecting pores in both the CAHA2A and CAHA2AP hydrogels (Figures 2H and 2K). Additionally, elemental analysis on both scaffolds revealed the level of different elements on the surface. As expected, the level of carbon, oxygen, and calcium predominated on both CAHA2A and CAHA2AP hydrogels. The level of calcium was increased over oxygen in CAHA2A whereas the reverse trend was observed in CAHA2AP. Surprisingly, the level of calcium predominated in CAHA2AP compared to CAHA2A and the sodium was detected in CAHA2A which was absent in CAHA2AP suggesting the increased crosslinking in CAHA2AP (Figures 2I and 2L).

Surface hydrophilicity—Contact angle measurements displayed similar values between the two scaffolds (Table 1). The advancing and receding angles observed for CAHA2A were 68.12 ± 1.00° and 68.02 ± 1.06° respectively and that for CAHA2AP were 68.39 ± 1.55° and 67.76 ± 1.30° respectively (n = 6). Interestingly, the contact angle values revealed the

amphiphilic nature of the hydrogels and there was no significant difference between the amphiphilicity between the two hydrogels *(P=0.8831).*

Water profile—Both CAHA2A and CAHA2AP hydrogels exhibited significant water holding capacity (n = 4) displaying 853 ± 71.50% and 721 ± 21.00%, respectively (Table 1). The swelling profile for both hydrogels showed a statistically significant increase from 5 to 75 minutes in comparison to time 0 (*P<0.0001*) (Figures 3A and 3B). Additionally, the EWC was 89.3 ± 0.79% for CAHA2A and 87.8 ± 0.31% for CAHA2AP suggesting the superabsorbent hydrogels (Table 1). Moreover, both hydrogels exhibited similar level of water holding capacity (*P=0.1269*) and EWC (*P=0.1213*). Also, the diffusional exponent (n) was −0.003 for CAHA2A and −0.014 for CAHA2AP whereas the swelling constant (k) was 0.975 for CAHA2A and 0.9131 for CAHA2AP (Table 1) (Figures 3A and 3B). Additionally, total water absorption sites (TWAS) was $4.63\times10^{24} \pm 8.40 \times10^{23}$ for CAHA2A and $2.50\times10^{24} \pm 2.87 \times10^{23}$ for CAHA2AP (Table 1) (Figures 3A and 3B).

Thermal analysis—The DSC cooling curves for both CAHA2A and CAHA2AP hydrogels displayed respective exothermic peaks due to crystallization of freezing water, and the heating curves showed an endothermic peak due to the melting of frozen water (Figures 3C and 3D). The DSC thermograms of CAHA2A and CAHA2AP exhibited a sharp endothermic peak at around −0.224 and −0.137, respectively. Also, the freezing-free water (Wf) were 67.5% and 61.0% and non-freezing water content (Wnf) were 21.8% and 26.8% for CAHA2A and CAHA2AP hydrogels, respectively, as determined from the enthalpy of melting endotherm (Table 1) (Liberski et al., 2016).

Conductance—The conductance of CAHA2A (3.966 ± 0.17 MΩ) was significantly higher than that of CAHA2AP (2.933 ± 0.14 MΩ) (*P=0.0402*).

Biodegradation—CAHA2A and CAHA2AP showed decrease in the dry weight in week-1 when compared to the control; however, was statistically not significant (*P=0.2404 and P=0.0877*, respectively) (Figure 3E). CAHA2A significant decrease in dry weight in week-2 and week-3 when compared to the control (*P=0.0007, P=0.0007*, respectively). Similarly, CAHA2AP displayed significant drop in dry weight in week-2 (*P<0.0001*) and week-3 (*P<0.0001*) (Figure 3E). In addition, both hydrogels showed a progressive increase in pH (Figure 3F). The pH displayed statistically significant weekly increase when compared to the baseline pH of 7.8 measured at day 0 in both the hydrogels. Furthermore, the pH following five weeks was 8.5 ± 0.19 (*P=<0.0001)* and 8.4 ± 0.18 (*P=0.001)* for CAHA2A and CAHA2AP respectively (Figure 3F).

Mechanocompatibility—Tensile strength was 46.56 ± 3.43 kPa and 50.87 ± 3.32 kPa for CAHA2A and CAHA2AP, respectively. Also, the elongation at break was 18.85 ± 2.13% and 18.17 ± 1.31% kPa for CAHA2A and CAHA2AP, respectively. Moreover, the Youngs modulus was 567.35 ± 61.91 kPa and 583.92 ± 49.48 kPa for CAHA2A and CAHA2AP, respectively (Table 1).

Release profile—The short-term release of methylene blue dye CAHA2A hydrogel increased progressively from 1 hour to 8 hours compared to the baseline control. The

amount of released methylene blue was significantly increased at 2 hrs (*P=0.001*), 3 hrs (*P=0.003*), 4 hrs *(P=0.0015),* 5 hrs *(P=0.0019),* and 6 hrs (*P=0.0219*) compared to control; however, the increase was statistically not significant at 1 hrs (*P=5424*), 7 hrs (*P=0.3537*), and 8 hrs *(P=0.6155)* (Figure 3G). Similarly, the short-term dye release profile of CAHA2AP displayed increased release at 2 hrs *(P=<0.0001),* 3 hrs *(P=<0.0001),* 4 hrs *(P=<0.0001),* 5 hrs *(P=<0.0001),* 6 hrs *(P=<0.0001),* 7 hrs *(P=0.0045),* and 8 hrs *(P=0.0028)* when compared to control; however, the increase at 1 hour was statistically not significant *(P=0.0611)* (Figure 3G). The long-term release profile displayed decrease in dye release from 3 to 14 days for CAHA2A; however, the decrease at day-4 was statistically not significant (P=0.2303). In addition, the CAHA2AP hydrogel exhibited increased release at day-3 (*P=0.8009*) and day-4 (*P=0.2304*) compared to day-2; however, was statistically not significant. Moreover, the release profile from 5 days to 14 days revealed significant decrease compared to day-2 (Figure 3H).

Hemocompatibility—CAHA2A and CAHA2AP hydrogels showed minimal hemolysis compared to the control samples. The percentage hemolysis was 1.88 ± 0.15% for CAHA2A (P<0.0001) 1.92 ± 0.16% for CAHA2AP (P<0.0001). Also, no considerable difference in hemolysis was observed between CAHA2A and CAHA2AP (P=0.8523) (Table 1). Moreover, the RBCs in contact with CAHA2A and CAHA2AP hydrogels exhibited minimal aggregation and rouleau formation as evident by light microscopy (Figures 4A–4C).

Adsorption of serum proteins—The total protein adsorbed onto CAHA2A and CAHA2AP were 1.44 ± 0.15 μg/μl *(P=<0.0001)* and 1.752 ± 0.08 μg/μl (*P=<0.0001*) respectively which were significantly increased compared to the control (Table 1). Also, the CAHA2AP hydrogel displayed significant increase in the level of adsorbed proteins compared to CAHA2A (*P=0.0485*). The SDS-PAGE demonstrated the adsorption of albumin in both the hydrogels in comparison to the control (Figures 4E and 4F). The relative absorption of albumin was 2.693 ± 0.61 μg/μL, 9.027 ± 0.72 μg/μL (*P=0.0005*) and 9.795 ± 0.36 μg/μL (*P=<0.0001*) respectively for control, CAHA2A and CAH2AP. Moreover, no considerable difference in albumin adsorption was observed between CAHA2A and CAHA2AP (P=0.8523) (Table 1).

Cytocompatibility—Direct contact assay provided information on the proliferative potential and the morphological changes associated with H9c2 cells following direct exposure to the hydrogel templates. Cells exposed to both CAHA2A and CAHA2AP exhibited similar physical characteristics with no alterations in morphology and were proliferative similar to the control cells (Figures 4G–4I). Also, the health status of H9c2 cells on contact with the hydrogels was confirmed quantitatively through MTT assay which displayed 101.9 ± 1.89% (*P=0.3788*) and 89.61 ± 3.22% (*P=0.4216*) respectively for CAHA2A and CAHA2AP relative to the control; however, was statistically not significant. Moreover, the viability of cells exhibited in CAHA2A was higher than CAHA2AP (*P=0.9352*); however, was not statistically significant (Table 1). Additionally, MTT assays on H9c2 cells grown on the extracts of both hydrogels displayed the viability of 110.91 ± 12.58% *(P=0.3788)* 109.92 ± 7.14% *(P=0.4216)* respectively for CAHA2A and CAHA2AP

relative to the control. Moreover, similar level of viability was exhibited between CAHA2A and CAHA2AP (*P=0.9350*) suggesting the non-toxic nature of both hydrogels (Table 1).

Biological Performance

Long-term viability: Long-term viability of H9c2 cells survived on the interstices of CAHA2A and CAHA2AP hydrogels were assessed for a period of 20 days at 5 days interval. The CAHA2A showed decreased viability at day-10 when compared to day 5 (*P=0.1445)*; however, displayed increased viability at day-15 (*P=0.4115*) and day-20 (*P=0.3671*) compared to day-5; however, these alterations were statistically not significant. The CAHA2AP hydrogel showed significant decrease in viability on day-10, day-15, and day-20 when compared to day 5 (*P<0.0001*) (Figure 5A).

Cell migration: The anterograde migration of H9c2 cells from both the CAHA2A and CAHA2AP hydrogels towards the culture plate peaked around day-7 of initial seeding and attained full confluency by day-10. Interestingly, similar trend was observed for the anterograde migration of both the hydrogel (Figure 5B). Trans-well migration assay confirmed the anterograde migration of cells from both the hydrogel as evident from the DAPI staining across the membrane (Figure 5C and 5D). The penetration (retrograde migration) of H9c2 cells onto the CAHA2A and CAHA2AP hydrogels were evaluated using PKH67 staining which revealed the penetration depth of 211.52 ± 34.04 μm and 165.92 ± 11.48 μm for CAHA2A and CAHA2AP hydrogels respectively. The cell penetration predominated in both the hydrogels compared to the control whereas CAHA2A displayed increased penetration depth than CAHA2AP (Figures 6A–6D). Similarly, the rhodamine-phalloidin staining revealed the cell spreading and retrograde migration up to the depth of 185.48 ± 53.87μm and 112.5 ± 24.96μm for CAHA2A and CAHA2AP hydrogels respectively. The cell survival predominated in both hydrogels compared to the control whereas CAHA2A displayed increased penetration depth than CAHA2AP (Figures 6E–6H). Moreover, rhodamine-phalloidin staining revealed the colonization of the cells suggesting their well-being in both hydrogels.

ECM deposition—Both the CAHA2A and CAHA2AP hydrogels promoted the ECM production by the seeded H9c2 cells as evident by aniline blue staining (Figure 7A–7C). Additionally, the quantification of ECM deposition using direct red assay revealed that CAHA2A displayed 1.29 ± 0.21% increase on day 5 (*P=0.0011*), 2.80% ± 0.15% increase on day 10 (*P=<0.0001*), and 1.84 ± 0.23% increase on day 15 (*P=0.0009*) whereas CAHA2AP hydrogels displayed 0.77 ± 0.18% increase on day 5 (*P=0.0058*), 1.78 ± 0.39% increase on day 10 (*P=0.0105*), and 1.88 ± 0.08% increase on day 15 (*P=<0.*0001) compared to the control; however, was not statistically significant between the two hydrogels (Table 1).

Co-culture—The EATDS and CF cells were harvested and characterized based on the immunopositivity of specific biomarkers (Thankam et al., 2022b) (data not shown in this article) and were labelled with viable fluorescent dyes displaying green and red fluorescence. Both the hydrogels supported the co-existence of EATDS and CF and exhibited the retrograde migration of the cells (EAT in green and CF in red) which was confirmed via z-stacks and 3D rendering (Figure 7D–7I) (Supplementary videos 1–3).

Interestingly, the CAHA2AP hydrogel revealed increased migration (59.59 ± 7.16μm) than CAHA2A 51.13 ± 5.24 μm; however, was not statistically significant (*P=0.3629*). Moreover, the cell penetration exhibited by the hydrogels predominated when compared to the control (*P=<0.0001* for CAHA2A and *P=0.0001* for CAHA2AP).

Discussion

The present study focused on the physiochemical and biological performance of novel hybrid IPN hydrogels synthesized from alginate, CMC, PVA, and HEMA for CTE applications. Alginate, a naturally occurring polysaccharide, form hydrogels in milder chemical reactions which has been used in immobilizing seeded cells for tissue engineering applications (Liberski et al., 2016). Cytosolic Ca^{++} ions play a critical role in the regulation of cardiomyocyte function. In normal physiology, Ca^{++} is predominantly introduced to the cardiac system though activation of ryanodine receptors (RyRs) and release from the sarcoplasmic reticulum (SR), which activates cross bridges between myofilament proteins leading to contraction. Impaired Ca^{++} homeostasis is a key feature of heart failure, contributing to contractile dysfunction and arrhythmias (Luo and Anderson, 2013) as the loss of Ca^{++} is detrimental to the performance of cardiomyocytes. Hence, the availability of additional Ca^{++} potentially assists in resolving the impaired homeostasis, providing a supplemental source of Ca^{++} to allow for normal cross bridge formation and contraction of the heart. Therefore, the Ca^{++} released by alginate dissociation from both the hydrogels benefits the cardiac function. Similarly, CMC is a polysaccharide creating a hydrated environment and promoting cell adhesion without eliciting any adverse biological responses (Namkaew et al., 2021). Also, PVA is a FDA-approved non-biodegradable synthetic polymer that provides appreciable good tensile and tear strength, and flexibility in biomaterial implants (Nuttelman et al., 2002; Pushp et al., 2021). However, PVA exhibits rapid disintegration in aqueous environment due to its extreme hydrophilicity which is combated through the stabilizing effect of co-polymers including alginate.

Generally, the tissue engineering hydrogels provide mechanical support for seeded cells to allowing them to deposit ECM and synthesize new tissue (Camci-Unal et al., 2014). Also, the mechanical compliance and swelling are controlled by the crosslinking density within the polymer networks, which reflect the thermodynamic stability of the hydrogels (Camci-Unal et al., 2014). As previously reported, the Young's modulus of a healthy human heart is typically below 50kPa; however, it increases up to 100 kPa under pathologic conditions, such as scarring and fibrosis (Allijn et al., 2020). Hence, in order to comply with the healing responses and beating function, the tissue engineering scaffolds require the mechanical properties greater to the native heart tissue as biodegradation declines the mechanical properties. Interestingly, both the hydrogels exhibited Youngs modulus over 500kPa, reflecting its high elasticity and ability to adapt to cardiac contraction. Hence, the co-polymer components of both CAHA2A and CAHA2AP scaffolds were proven to be advantageous for the survival and proliferation of H9c2 cells as evident from the hydrophilic, mechanical and biocompatible nature. Additionally, the hydrogel components CMC, HEMA, alginate, and AA were reported to be biocompatible, and have been exploited for multitude of biomedical applications (El-Sherbiny and Yacoub, 2013). Interestingly, the reinforcement with PVA imparted additional strength of the CAHA2AP hydrogel and

is advantageous owing to its adhesive and emulsifying properties (Jensen et al., 2016). Additionally, the superior porosity exhibited by CAHA2A and CAHA2AP benefited the acquisition of water molecules onto their networks as evident from the swelling kinetics satisfying to be classified as superabsorbent.

Superabsorbent hydrogels are characterized by the superior water content and holding capability, which is controlled by the diffusion, as discussed previously (Thankam et al., 2022a). Diffusion is controlled by the diffusional exponent (n), which favors the movement of water via Fickian diffusion (controlled by swelling), or Super Case II Transport (SCIIT) (controlled by network relaxation). Swelling follows Fickian diffusion when $n \leq 0.5$m and follows SCIIT when $n \geq 1.0$ (Pushp et al., 2021). Both hydrogels have shown to have $n \leq 0.5$m, meaning that they both follow Fickian diffusion. Fickian diffusion is related to the diffusive flux or the amount of substance per unit area per unit time, which in turn related to the TWAS found within these hydrogels. The high amounts of TWAS on both hydrogels allow for increased uptake of water within a short period of time. This was reflected in swelling studies with a significant increase of around 840% and 740% swelling of the CAHA2A and CAHA2AP hydrogels, respectively, after only five minutes of submersion in water. Additionally, the hydrophilicity of the hydrogels is due to the distribution of hydrophilic functional groups of the backbone of the polymers including carboxyl, amide, amino, and hydrohyl groups (El-Sherbiny, 2013). Hence, the hydrophilicity allows the intake of water molecules and the controlled release of loaded molecules. In addition, the biomolecules involved in the cellular performance on the hydrogels possess amphiphilic domains suggesting the presence of both hydrophilic and hydrophobic moieties. Interestingly, the data on the release profile for the hydrophilic and hydrophobic dyes suggest the similar response of the hydrogels towards both hydrophilic and hydrophobic; however, further optimization is warranted for correlating the cellular responses with the findings from release kinetics.

In general, the homogenous porous architecture designed in the hydrogel templates facilitate the uniform distribution, adhesion, growth, proliferation, and migration of seeded cells which are crucial for successful CTE (El-Sherbiny and Yacoub, 2013). Interestingly, the previous studies demonstrated the minimum requirement of micro-scale pore length (typically >80μm) at an equilibrium swollen state is essential for accelerated cell migration, angiogenesis and metabolite trafficking (Annabi et al., 2010; Ashtaputrey and Ashtaputrey, 2018). The current study shows porosity (aspect ratio) of ~1.40μm which has shown to be smaller than the requirments. Interestingly, the data presented in the present study used freeze dried hydrogels and the swelling in the medium opens the pores and favors superior pore interconnectivity. Also, the optimum pore size for neovascularization is 5μm, and 5–15μm for fibroblast ingrowth (Annabi et al., 2010) which would be facilitated by swelling. Hence, the hydrogels are optimal for cell migration in vivo, neovascularization and fibroblast ingrowth allowing the adhesion and survival of seeded cells, while the controlled degredation of the hydrogels facilitates the release of loaded cells or mediators. Additionally, the porosity contributes to the surface roughness increasing the surface area allowing the 3D growth of the seeded cells (Gnanaprakasam Thankam and Muthu, 2014). Interestingly, the surface roughness of CAHA2A predominated than CAHA2AP; however, both the hydrogels

promoted the growth and migration of H9c2 cells suggesting their potential application in CTE.

The biodegradable scaffolds ensure the timely replacement of the hydrogel/implant in proportionate with the growth and regeneration of tissue.

Both the CAHA2A and CAHA2AP hydrogels are biodegradable/bioerodable which in turn was tuned based on the reversible sol-gel crosslinking chemistry of alginate through the exchange of divalent ions with monovalent ions (Thankam et al., 2022a). The Ca^{++} cross linked alginate gel transforms to solution form upon exchange of Ca++ with monovalent Na+ ions from the media which disturbs the molecular architecture of the hydrogel altering the crosslinking density owing to the further influx of water molecules. Hence, the dissociation of alginate fraction from the hydrogel surface facilitates the degradation machinery to access the inner molecular layers of the hydrogel contributing to the erosion of hydrogel fragments depending on the crosslinking density. Moreover, the slight increase in pH following biodegradation of CAHA2A and CAHA2AP hydrogels reflected the mildly basic degradation products which are possibly be neutralized and cleared post implantation though physiologic buffers and circulatory fluids. Importantly, the degradation products released from CAHA2A and CAHA2AP were non-toxic as evident from the increased viability of H9c2 cells by MTT and direct contact assay suggesting the minimal toxicity of these hydrogels in CTE.

RBC aggregation upon the contact of scaffolds with circulatory fluids leads to low sheer blood viscosity and microvascular flow dynamics, resulting in hemodynamic adverse effects (Ashtaputrey and Ashtaputrey, 2018; El-Sherbiny and Yacoub, 2013). Both the CAHA2A and CAHA2AP hydrogels displayed minimal aggregation and morphological alterations of RBC and hemolysis suggesting their hemocompatibility. In addition, CAHA2AP promoted increased protein absorption, particularly albumin, in comparison to the CAHA2A scaffold, despite their similar hydrophilicity (Gnanaprakasam Thankam et al., 2013). Importantly, the adsorption of albumin favors the the passivation effect promoting biocompatibility and cell adhesion owing to the formation of a provisional matrix for the cell survival (Rampling et al., 2004). Moreover, the albumin coatings in biomaterials implants induce thromboresistive effect preventing the clot formation and inflammatory responses (Law, 2014). Moreover, the porosity, hydrophilicity and distribution of water molecules in the hydrogel interstitial spaces modulating the protein adsorption (Chien et al., 2017; El-Sherbiny and Yacoub, 2013; Gonçalves et al., 2009; Hanein et al., 1993). Our data on CAHA2A and CAHA2AP hydrogels reflected from the physiochemical properties, RBC aggregation assay and the extent of albumin adsorption suggest the safer application in vivo.

CAHA2A and CAHA2AP hydrogels are cytocompatibile allowing the H9c2 cell adhesion, proliferation, and survival. Also, both the hydrogels retained the viability >80% after 15 days suggesting the potential of the hydrogels to promote the suatainence and survival of cardiac cells. However, the extent of viability was higher in CAHA2A hydrogels compared to CAHA2AP owing to the decreased porosity as the viability of proliferating cells significantly depends on the extent of porosity (Gnanaprakasam Thankam and Muthu, 2014). Furthermore, the bidirectional migration (anterograde and retrograde) of the cells

exhibited by CAHA2A and CAHA2AP hydrogels is crucial for the migration of seeded cells towards and the host cells from the surviving cardiac tissue post-implantation. Moreover, the cells infiltrated ~110μm within the CAHA2A scaffolds, traveling through the highly porous structures suggesting the potential of the proliferating cells to occupy the inner rooms of the hydrogel (Ishihara et al., 1998). Additionally, the biodegradation facilitates ample space for the proliferating cells within the scaffolds. Furthermore, the flux of the seeded cells toward the periphery and out the scaffolds resulted in increased cell density at the interface suggesting the potential applications of the hydrogels in cell delivery for cardiac regeneration. Moreover, the CAHA2A and CAHA2AP hydrogels promoted the ECM deposition onto their interstices allowing the cells to establish colonies eventually leading to the formation of neocardiac tissue (Frangogiannis, 2019; Rienks et al., 2014).

The successful CTE largely depends on the co-existence and communication of multiple primary cell types associated with cardiac healing. For instance, the CFs are responsible for ECM restoration within the surviving myocardium crucial for cardiac healing (MacKenna, 2000). In addition, the stem cells from adjacent locations including the epicardial adipose tissue (EAT) communicate with the ischemic myocardium triggering the activation of EATDS facilitating their differentiation towards cardiac lineages (Özkaynak et al., 2021; Thomson et al., 1998). Co-culture experiments ensured the co-existence of CFs and EATDS under in vitro conditions in a 3D environment provided by both the hydrogels suggesting the translational potential of the hydrogels for cardiac applications.

Overall, both the CAHA2A and CAHA2AP scaffolds have shown to be promising in the delivery of cells to the local environment promoting both anterograde and retrograde movement. In addition, the CAHA system warrants further in vitro and in vivo investigations in translationally relevant experimental models for the optimization of the scaffolds pre- and post-implantation. The future application of the CAHA2A and CAHA2AP in CTE utilizing CF and EATDS will facilitate myocardial repair and regeneration. Hence, we anticipate that these hydrogels (owing to the encouraging features) facilitate the replenishment of the cells into the target site. Further in-depth investigations using in vivo translational models are warranted for the validation of the hydrogels for clinical cardiology. Despite the encouraging findings, the major limitation of the study is the lack of explanation regarding the adsorbed proteins other than albumin, in vivo evaluations, and implantation strategies for clinical applications. Nonetheless, the present study reflects the promising translational significance of CAHA2A and CAHA2AP scaffold systems for MI management.

Conclusions

CAHA2A and CAHA2AP hydrogels were synthesized by IPN chemistry which exhibited superior physiochemical features, porosity, tensile strength, hydrophilicity, water profiling, and biodegradation. The hydrogels were hemocompatibile and cytocompatibility studies and facilitated the adsorption of plasma proteins especially albumin. Additionally, the hydrogels supported the adhesion and colonization of cells, bidirectional movement, co-existance of EATDS and CF cells and ECM deposition which are crucial for viable CTE. Overall, both CAHA2A and CAHA2AP hydrogels exhibit promising translational potential towards the engineering and regeneration of cardiac tissue.

Supplementary Material

Refer to Web version on PubMed Central for supplementary material.

References

Allijn I, Ribeiro M, Poot A, Passier R, Stamatialis D. Membranes for Modelling Cardiac Tissue Stiffness In Vitro Based on Poly(trimethylene carbonate) and Poly(ethylene glycol) Polymers. Membranes (Basel). 2020 Oct 3;10(10):274. doi: 10.3390/membranes10100274. [PubMed: 33022962]

Annabi N, Nichol JW, Zhong X, Ji C, Koshy S, Khademhosseini A, Dehghani F. 2010. Controlling the Porosity and Microarchitecture of Hydrogels for Tissue Engineering. Tissue Eng. Part B Rev. 16:371–383. [PubMed: 20121414]

Ashtaputrey P, Ashtaputrey S. 2018. STUDY OF SWELLING BEHAVIOR AND DETERMINATION OF SWELLING PARAMETERS OF SPHERICAL HYDROGELS IN WATER. J. Drug Deliv. Ther. 8:218–222.

Aswathy SH, Narendrakumar U, & Manjubala I 2020. Commercial hydrogels for biomedical applications. Heliyon, 6(4), e03719. [PubMed: 32280802]

Bahit MC, Kochar A, Granger CB. 2018. Post-Myocardial Infarction Heart Failure. JACC Heart Fail. 6:179–186. [PubMed: 29496021]

Camci-Unal G, Annabi N, Dokmeci MR, Liao R, Khademhosseini A. 2014. Hydrogels for cardiac tissue engineering. NPG Asia Mater. 6:e99–e99.

Chien S-C, Chen C-Y, Lin C-F, Yeh H-I. 2017. Critical appraisal of the role of serum albumin in cardiovascular disease. Biomark. Res. 5:31. [PubMed: 29152305]

Dunlay SM, Weston SA, Jacobsen SJ, Roger VL. 2009. Risk Factors for Heart Failure: A Population-Based Case-Control Study. Am. J. Med. 122:1023–1028. [PubMed: 19854330]

El-Sherbiny IM, Yacoub MH. 2013. Hydrogel scaffolds for tissue engineering: Progress and challenges. Glob. Cardiol. Sci. Pract. 2013:38.

Finosh GT, Jayabalan M. 2015. Hybrid amphiphilic bimodal hydrogels having mechanical and biological recognition characteristics for cardiac tissue engineering. RSC Adv. 5:38183–38201.

Finosh GT, Jayabalan M, Vandana S, Raghu KG. 2015. Hybrid alginate-polyester bimodal network hydrogel for tissue engineering – Influence of structured water on long-term cellular growth. Colloids Surf. B Biointerfaces 135:855–864. [PubMed: 25843368]

Frangogiannis NG. 2019. The Extracellular Matrix in Ischemic and Nonischemic Heart Failure. Circ. Res. 125:117–146. [PubMed: 31219741]

Gnanaprakasam Thankam F, Muthu J. 2013. Influence of plasma protein–hydrogel interaction moderated by absorption of water on long-term cell viability in amphiphilic biosynthetic hydrogels. RSC Adv. 3:24509.

Gnanaprakasam Thankam F, Muthu J. 2014. Alginate based hybrid copolymer hydrogels—Influence of pore morphology on cell–material interaction. Carbohydr. Polym. 112:235–244. [PubMed: 25129740]

Gnanaprakasam Thankam F, Muthu J, Sankar V, Kozhiparambil Gopal R. 2013. Growth and survival of cells in biosynthetic poly vinyl alcohol–alginate IPN hydrogels for cardiac applications. Colloids Surf. B Biointerfaces 107:137–145. [PubMed: 23475061]

Gonçalves IC, Martins MCL, Barbosa MA, Ratner BD. 2009. Protein adsorption and clotting time of pHEMA hydrogels modified with C18 ligands to adsorb albumin selectively and reversibly. Biomaterials 30:5541–5551. [PubMed: 19595453]

Gustafsson F, Rogers JG. 2017. Left ventricular assist device therapy in advanced heart failure: patient selection and outcomes: LVAD therapy in HF. Eur. J. Heart Fail. 19:595–602. [PubMed: 28198133]

Hanein D, Geiger B, Addadi L. 1993. Fibronectin adsorption to surfaces of hydrated crystals. An analysis of the importance of bound water in protein-substrate interactions. Langmuir 9:1058–1065.

Heidenreich PA, Albert NM, Allen LA, Bluemke DA, Butler J, Fonarow GC, Ikonomidis JS, Khavjou O, Konstam MA, Maddox TM, Nichol G, Pham M, Piña IL, Trogdon JG. 2013. Forecasting the Impact of Heart Failure in the United States: A Policy Statement From the American Heart Association. Circ. Heart Fail. 6:606–619. [PubMed: 23616602]

Ishihara K, Nomura H, Mihara T, Kurita K, Iwasaki Y, Nakabayashi N. 1998. Why do phospholipid polymers reduce protein adsorption? J. Biomed. Mater. Res. 39:323–330. [PubMed: 9457564]

Jensen BEB, Dávila I, Zelikin AN. 2016. Poly(vinyl alcohol) Physical Hydrogels: Matrix-Mediated Drug Delivery Using Spontaneously Eroding Substrate. J. Phys. Chem. B 120:5916–5926. [PubMed: 26958864]

Law K-Y. 2014. Definitions for Hydrophilicity, Hydrophobicity, and Superhydrophobicity: Getting the Basics Right. J. Phys. Chem. Lett. 5:686–688. [PubMed: 26270837]

Li Z, Guan J. Hydrogels for Cardiac Tissue Engineering. Polymers. 2011; 3(2):740–761. 10.3390/polym3020740

Liberski A, Latif N, Raynaud C, Bollensdorff C, Yacoub M. 2016. Alginate for cardiac regeneration: From seaweed to clinical trials. Glob. Cardiol. Sci. Pract. 2016. https://globalcardiologyscienceandpractice.com/index.php/gcsp/article/view/6.

Luo M, & Anderson ME 2013. Mechanisms of altered Ca^{2+} handling in heart failure. Circulation research, 113(6), 690–708. [PubMed: 23989713]

MacKenna D 2000. Role of mechanical factors in modulating cardiac fibroblast function and extracellular matrix synthesis. Cardiovasc. Res. 46:257–263. [PubMed: 10773229]

Minicucci MF, Azevedo PS, Polegato BF, Paiva SAR, Zornoff LAM. 2011. Heart Failure After Myocardial Infarction: Clinical Implications and Treatment. Clin. Cardiol. 34:410–414. [PubMed: 21688276]

Namkaew J, Laowpanitchakorn P, Sawaddee N, Jirajessada S, Honsawek S, Yodmuang S. 2021. Carboxymethyl Cellulose Entrapped in a Poly(vinyl) Alcohol Network: Plant-Based Scaffolds for Cartilage Tissue Engineering. Molecules 26:578. [PubMed: 33499342]

Nuttelman CR, Henry SM, Anseth KS. 2002. Synthesis and characterization of photocrosslinkable, degradable poly(vinyl alcohol)-based tissue engineering scaffolds. Biomaterials 23:3617–3626. [PubMed: 12109687]

Özkaynak B, Şahin İ, Özenc E, Subaşı C, Oran DS, Totoz T, Tetikkurt ÜS, Mert B, Polat A, Okuyan E, Karaöz E. 2021. Mesenchymal stem cells derived from epicardial adipose tissue reverse cardiac remodeling in a rabbit model of myocardial infarction. Eur. Rev. Med. Pharmacol. Sci. 25:4372–4384. [PubMed: 34227072]

Pushp P, Bhaskar R, Kelkar S, Sharma N, Pathak D, Gupta MK. 2021. Plasticized poly(vinylalcohol) and poly(vinylpyrrolidone) based patches with tunable mechanical properties for cardiac tissue engineering applications. Biotechnol. Bioeng. 118:2312–2325. [PubMed: 33675237]

Rampling MW, Meiselman HJ, Neu B, Baskurt OK. 2004. Influence of cell-specific factors on red blood cell aggregation. Biorheology 41:91–112. [PubMed: 15090679]

Rana A, Gruessner A, Agopian VG, Khalpey Z, Riaz IB, Kaplan B, Halazun KJ, Busuttil RW, Gruessner RWG. 2015. Survival Benefit of Solid-Organ Transplant in the United States. JAMA Surg. 150:252. [PubMed: 25629390]

Rienks M, Papageorgiou A-P, Frangogiannis NG, Heymans S. 2014. Myocardial Extracellular Matrix: An Ever-Changing and Diverse Entity. Circ. Res. 114:872–888. [PubMed: 24577967]

Thankam FG, Agrawal DK. 2022. Single Cell Genomics Identifies Unique Cardioprotective Phenotype of Stem Cells derived from Epicardial Adipose Tissue under Ischemia. Stem Cell Rev. Rep. 18:294–335. [PubMed: 34661829]

Thankam FG, Diaz C, Chandra I, Link J, Newton J, Dilisio MF, Agrawal DK. 2022a. Hybrid interpenetrating hydrogel network favoring the bidirectional migration of tenocytes for rotator cuff tendon regeneration. J. Biomed. Mater. Res. B Appl. Biomater. 110:467–477. [PubMed: 34342931]

Thankam FG, Huynh J, Fang W, Chen Y, Agrawal DK. 2022b. Exosomal-ribosomal proteins-driven heterogeneity of epicardial adipose tissue derived stem cells under ischemia for cardiac regeneration. J. Tissue Eng. Regen. Med:term.3289.

Thankam FG, Muthu J. 2014a. Influence of physical and mechanical properties of amphiphilic biosynthetic hydrogels on long-term cell viability. J. Mech. Behav. Biomed. Mater. 35:111–122. [PubMed: 24762858]

Thankam FG, Muthu J. 2014b. Infiltration and sustenance of viability of cells by amphiphilic biosynthetic biodegradable hydrogels. J. Mater. Sci. Mater. Med. 25:1953–1965. [PubMed: 24845306]

Thomson JA, Itskovitz-Eldor J, Shapiro SS, Waknitz MA, Swiergiel JJ, Marshall VS, Jones JM. 1998. Embryonic Stem Cell Lines Derived from Human Blastocysts. Science 282:1145–1147. [PubMed: 9804556]

Tsao CW, Aday AW, Almarzooq ZI, Alonso A, Beaton AZ, Bittencourt MS, Boehme AK, Buxton AE, Carson AP, Commodore-Mensah Y, Elkind MSV, Evenson KR, Eze-Nliam C, Ferguson JF, Generoso G, Ho JE, Kalani R, Khan SS, Kissela BM, Knutson KL, Levine DA, Lewis TT, Liu J, Loop MS, Ma J, Mussolino ME, Navaneethan SD, Perak AM, Poudel R, Rezk-Hanna M, Roth GA, Schroeder EB, Shah SH, Thacker EL, VanWagner LB, Virani SS, Voecks JH, Wang N-Y, Yaffe K, Martin SS, on behalf of the American Heart Association Council on Epidemiology and Prevention Statistics Committee and Stroke Statistics Subcommittee. 2022. Heart Disease and Stroke Statistics—2022 Update: A Report From the American Heart Association. Circulation 145. 10.1161/CIR.0000000000001052.

Vaduganathan M, Claggett BL, Jhund PS, Cunningham JW, Pedro Ferreira J, Zannad F, Packer M, Fonarow GC, McMurray JJV, Solomon SD. 2020. Estimating lifetime benefits of comprehensive disease-modifying pharmacological therapies in patients with heart failure with reduced ejection fraction: a comparative analysis of three randomised controlled trials. The Lancet 396:121–128.

Zin KM, Effendi Halmi MI, Abd Gani SS, Zaidan UH, Samsuri AW, & Abd Shukor MY 2020. Microbial Decolorization of Triazo Dye, Direct Blue 71: An Optimization Approach Using Response Surface Methodology (RSM) and Artificial Neural Network (ANN). BioMed research international, 2020, 2734135. [PubMed: 32149095]

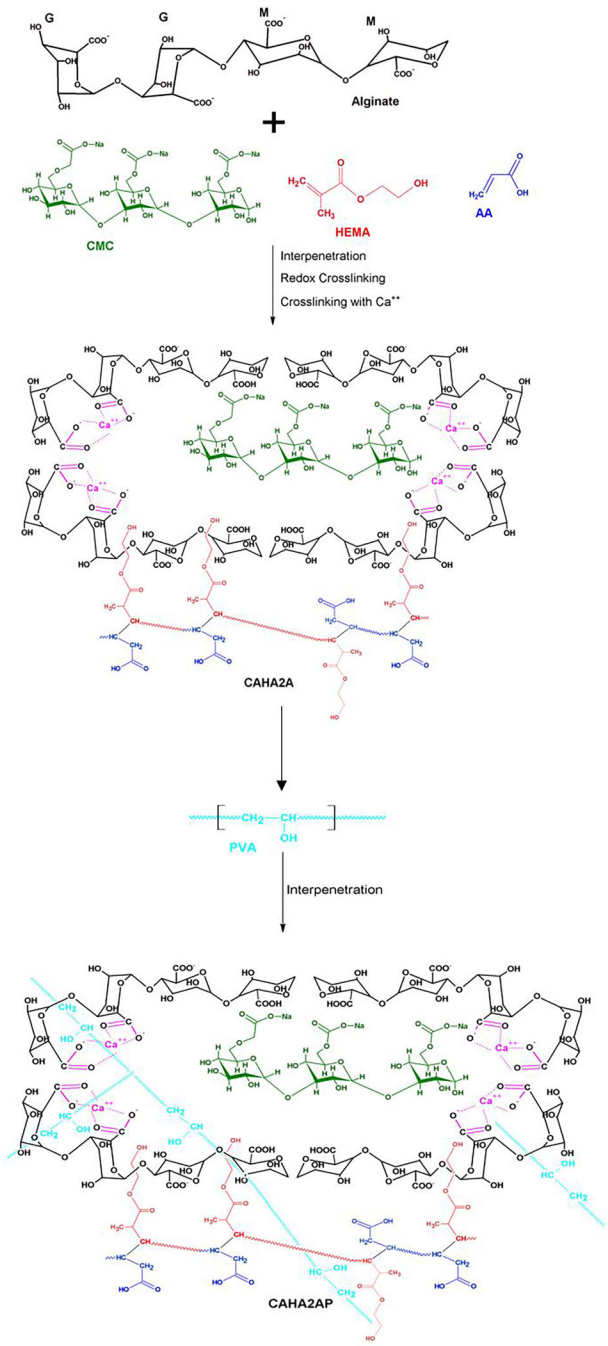

Figure 1:

Synthesis of interpenetrating network hydrogels CAHA2A and CAHA2AP using HEMA and alginate with ionic and vinyl cross-linking respectively. CAHA2AP hydrogels were further reinforced with PVA to provide additional stability to the scaffold.

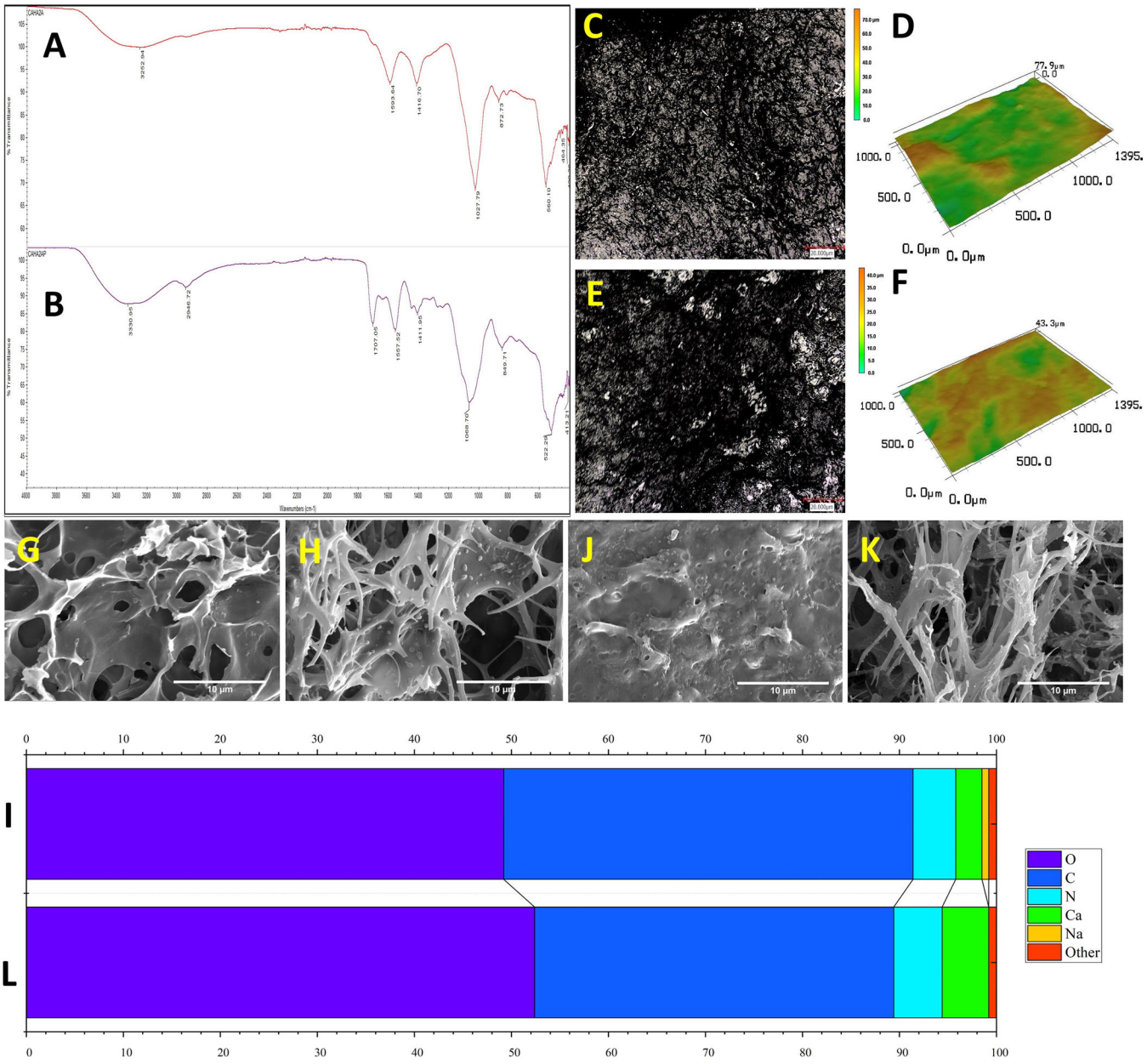

Figure 2:

(A) and (B) AT-IR of freeze-dried CAHA2A and CAHA2AP hydrogels. IR spectrum of the hydrogel scaffolds reveal the characteristic functional groups on the surface. (C) – (F) Surface imaging and 3D rendering of CAHA2A and CAHA2AP hydrogels. SEM analysis revealing the (G) surface and (H) inner porosity of CAHA2A hydrogel and (J) surface and (K) inner porosity of CAHA2AP hydrogel. (I) and (L) Map sum spectrum for the elemental analysis of CAHA2A and CAHA2AP.

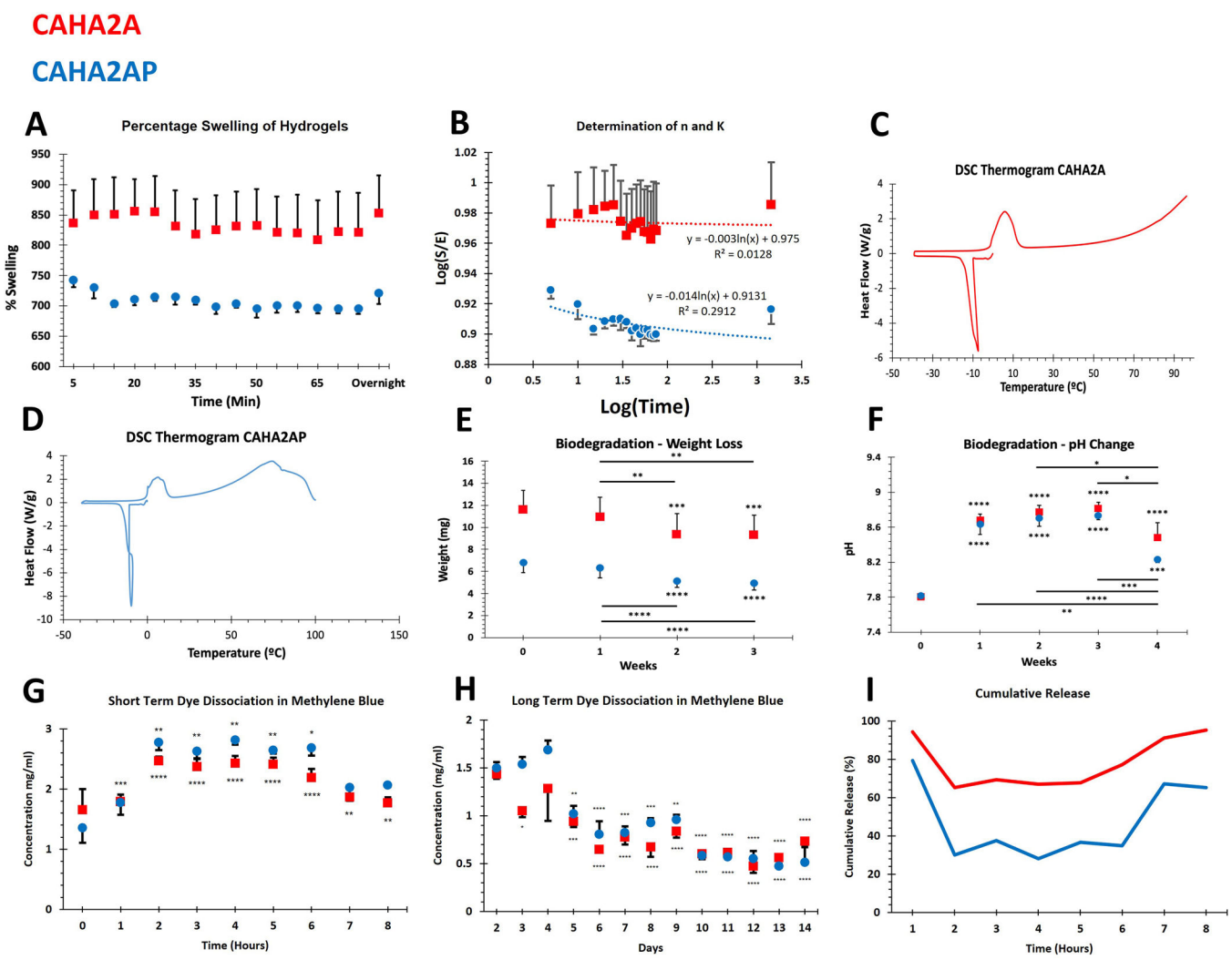

Figure 3:

(A) The swelling profile of CAHA2A and CAHA2AP hydrogels determined at an interval of 5 min for 75 minutes and overnight swelling. (B) Determination of diffusional exponent (n) and the swelling constant (K) from the plot of log(S/E) along the Y-axis and log(time) along the X-axis. (C) and (D) DSC thermogram of CAHA2A and CAHA2AP hydrogel showing the melting of freezing water. (E) – (F) Alterations in the dry weight and pH upon aging in DMEM for 4 weeks. (G) Short term dye dissociation of methylene blue from CAHA2A and CAHA2AP scaffolds. (H) Long term dye dissociation of methylene blue from CAHA2A and CAHA2AP scaffolds. *(*P< 0.05, **P< 0.01, ***P<0.001, ****P<0.0001, and unlabeled values are not significant*). (I) Short term cumulative release of methylene blue from CAHA2A and CAHA2AP scaffolds.

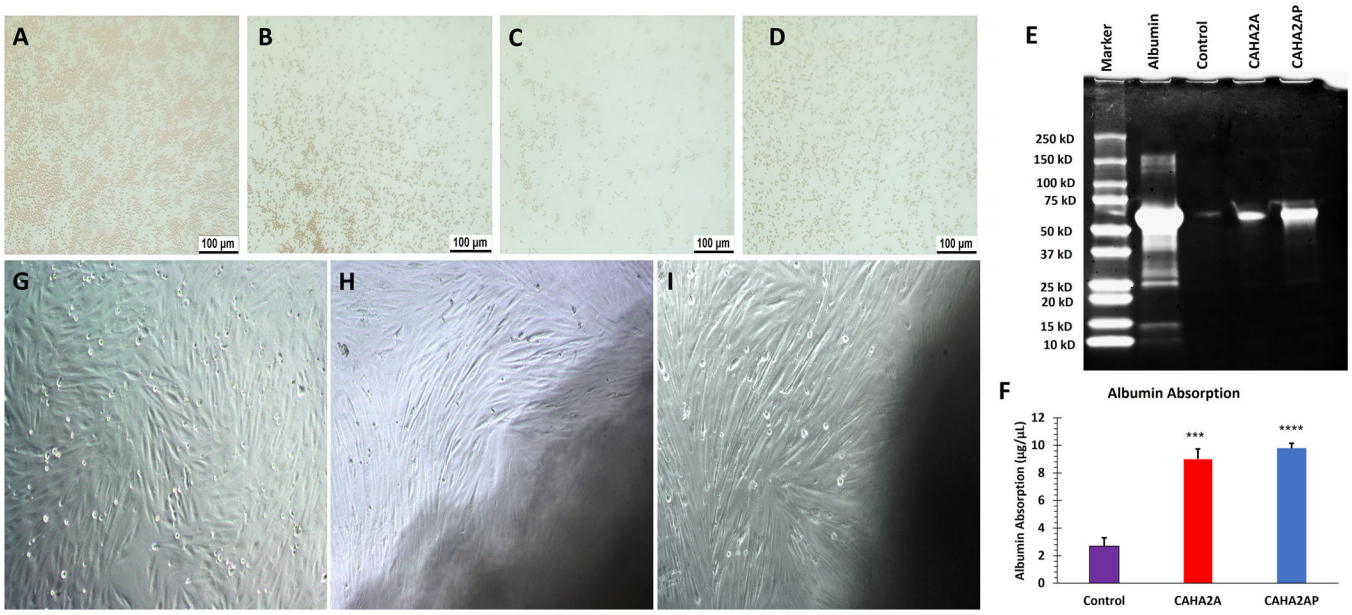

Figure 4:

Red Blood Cell Aggregation. (A) RBC solution water, (B) RBC solution in filtered PBS, CAHA2A (C) and CAHA2AP (D) samples. (E) SDS PAGE for albumin adsorption and (F) quantification of plasma protein adsorption extrapolated from the SDS PAGE using ImageJ. (G-I) The direct contact assay of H9c2 cells showing the absence of changes in cell morphology in the vicinity of CAHA2A scaffolds (H) and CAHA2AP scaffolds (I) when compared with control (G). Images were taken in 20X magnification under phase contrast microscope. *(*P< 0.05, **P< 0.01, ***P<0.001, ****P<0.0001, and unlabeled values are not significant*)

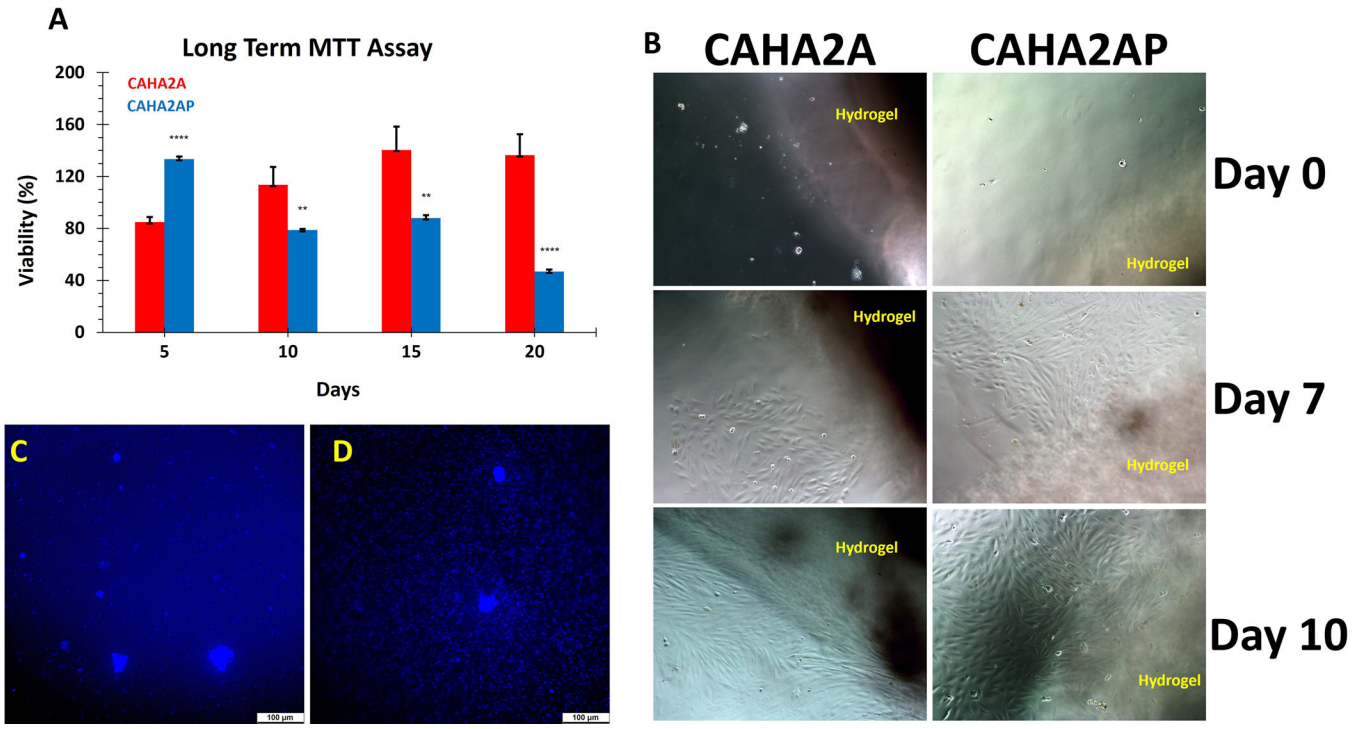

Figure 5:

(A) Evaluation of long-term cytotoxicity of CAHA2A and CAHA2AP scaffolds on H9c2 cells as determined by MTT assays. (B) Phase contrast imaging for the migration of H9c2 cells from the CAHA2A and CAHA2AP hydrogel to the culture plate. Cell migration from the hydrogel scaffolds were imaged on the day of seeding (Day 0) and day 7 and day 10 post-seeding. Images were taken in 20X magnification under phase contrast microscope. (C) – (D) Transwell migration of H9c2 cells seeded onto CAHA2A (C) and CAHA2AP (D) hydrogels after 3 days of initial seeding. Membranes were then stained with DAPI and imaged using fluorescent microscope at 20x. *(*P< 0.05, **P< 0.01, ***P<0.001, ****P<0.0001, and unlabeled values are not significant*)

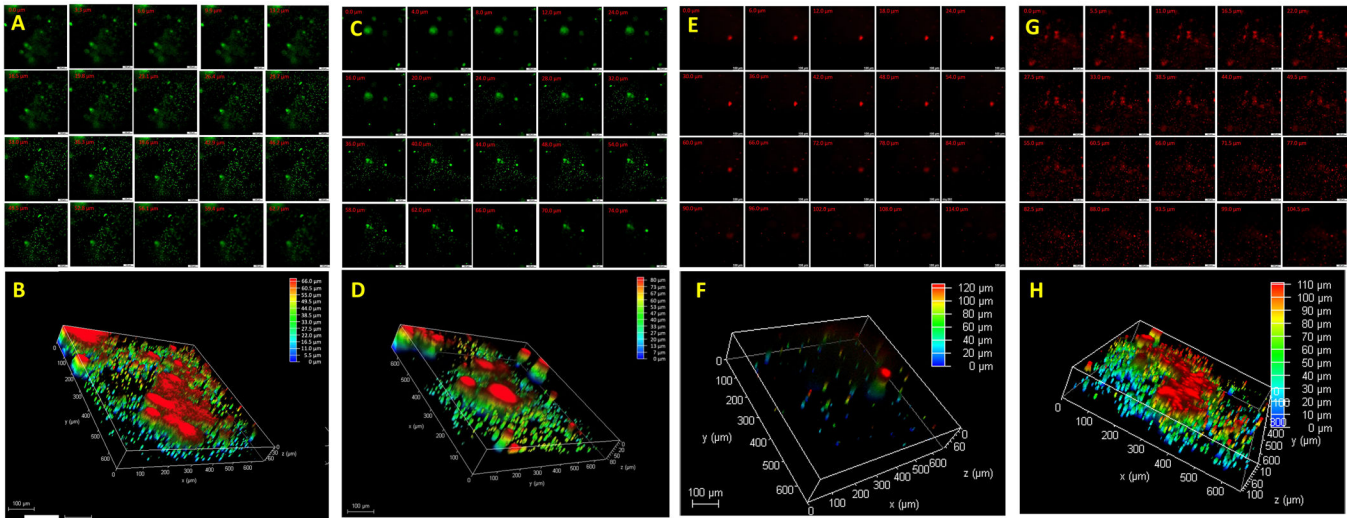

Figure 6:

(A) – (D) The gallery images of Z-stacks representing the infiltration of H9c2 cells stained with PKH67 toward the interior of CAHA2A scaffolds (A) and CAHA2AP scaffolds (B). 3D renders of CAHA2A (C) and CAHA2AP (D) obtained through the overlay of Z-stacks, allowing for the visualization of penetration depth of the H9c2 cells. (E) – (H) The gallery images of Z-stacks representing the infiltration of H9c2 cells toward the interior of CAHA2A scaffolds (E) and CAHA2AP scaffolds (F) stained with Rhodamine Phalloidin 3 days post-seeding. 3D renders of CAHA2A (G) and CAHA2AP (H) obtained through the overlay of Z-stacks, allowing the visualization of penetration depth of the H9c2 cells.

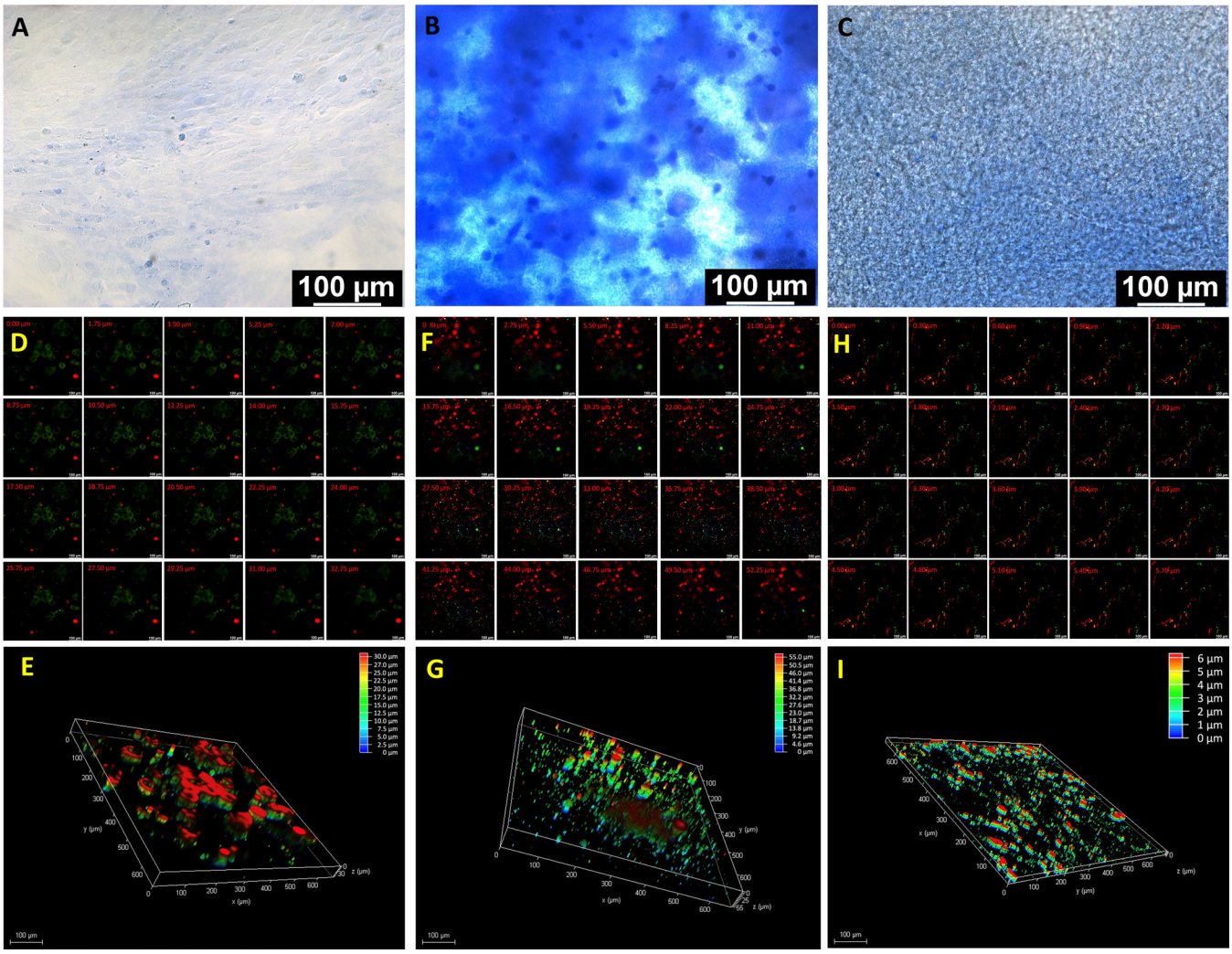

Figure 7:

(A-C) Collagen staining with aniline blue. (A) Control H9C2 cells. (B) CAHA2A seeded with H9C2 cells. (C) CAHA2AP seeded with H9C2 cells. Images were taken in 20X magnification under phase contrast microscope. (D-G) The gallery images of Z-stacks representing the infiltration of H9C2 cells stained in PKH 26 (red) and EAT cells stained in PKH 67 (green) toward the interior of CAHA2A scaffolds (D) and CAHA2AP scaffolds (F). Additionally, Hoechst was used to stain cell nuclei. 3D renders of cell penetration into CAHA2A (E) and CAHA2AP (G) were obtained through the overlay of Z-stacks. Control EAT and CF cells were similarly imaged (H) and overlayed to create a 3D render (I).

Table 1:

Characteristic features of CAHA2A and CAHA2AP.

Parameters	CAHA2A	CAHA2AP	P Value
Physical properties			
Surface porosity (μm) (n = 7)	1.41 ± 0.09	1.34 ± 0.08	0.5864
Inner porosity (μm) (n = 7)	1.34 ± 0.06	1.46 ± 0.06	0.2053
Contact angle (deg) – advancing (n = 6)	68.12 ± 1.00	68.39 ± 1.55	0.8831
Contact angle (deg) – receding (n = 6)	68.02 ± 1.06	67.76 ± 1.30	0.8832
Swelling (%) (n = 4)	853 ± 71.50	721 ± 21.00	0.1269
Equilibrium water content (EWC) (%) (n = 4)	89.3 ± 0.79	87.8 ± 0.31	0.1213
Total Water Absorption Sites (TWAS) (n = 4)	$4.63 \times 10^{24} \pm 8.40 \times 10^{23}$	$2.50 \times 10^{24} \pm 2.87 \times 10^{23}$	0.0737
Diffusional exponent (n) (n = 4)	-3.00×10^{-3}	-1.40×10^{-3}	n/a
Swelling constant (k) (n = 4)	0.975	0.9131	n/a
Thermal properties			
Enthalpy of melting endotherm (J/g)	225.5	203.6	n/a
Freezing water content (*W*f) (%)	67.5	61.0	n/a
Non-freezing water content (*W*nf) (%)	21.8	26.8	n/a
Electrical properties			
Conductance (MΩ) (n = 6)	3.97 ± 0.17	2.93 ± 0.14	0.0402
Mechanical properties			
Tensile strength (kPA) (n = 5)	46.56 ± 3.43	50.87 ± 3.32	0.7137
Elongation at break (%) (n = 5)	18.85 ± 2.13	18.71 ± 1.31	0.9942
Young's modulus (kPa) (n = 5)	567.35 ± 61.91	583.92 ± 49.48	0.8396
Hemocompatibility			
Hemolysis (%) (n = 3)	0.60 ± 0.16	0.64 ± 0.16	0.8808
Absorption of protein (μg/μL) (n = 3)	1.44 ± 0.15	1.75 ± 0.08	0.0485
Albumin adsorption (μg/μL) (n = 3)	9.15 ± 0.53	9.89 ± 0.15	0.2380
Cytocompatibility			
Direct contact viability (%) (n = 6)	101.48 ± 1.89	89.61 ± 3.22	0.0131

Parameters	CAHA2A	CAHA2AP	P Value
Test on extract (%) (n = 4)	110.91 ± 12.58	109.92 ± 7.14	0.9352
Biologic Performance			
ECM content 5 days (%) (n = 4)	1.29 ± 0.21	0.77 ± 0.18	0.1135
ECM content 10 days (%) (n = 4)	2.80 ± 0.15	1.78 ± 0.39	0.0710
ECM content 15 days (%) (n = 4)	1.84 ± 0.23	1.88 ± 0.08	0.8769